EUKARYOTIC CELL, May 2010, p. 795–805 Vol. 9, No. 5
1535-9778/10/$12.00 doi:10.1128/EC.00058-10

Interaction of the *Aspergillus nidulans* Microtubule-Organizing Center (MTOC) Component ApsB with Gamma-Tubulin and Evidence for a Role of a Subclass of Peroxisomes in the Formation of Septal MTOCs[▽]

Nadine Zekert,‡ Daniel Veith,†‡ and Reinhard Fischer*

Karlsruhe Institute of Technology, Institute for Applied Biosciences, Department of Microbiology, Hertzstrasse 16, D-76187 Karlsruhe, Germany

Received 6 March 2010/Accepted 19 March 2010

Peroxisomes are a diverse class of organelles involved in different physiological processes in eukaryotic cells. Although proteins imported into peroxisomes carry a peroxisomal targeting sequence at the C terminus (PTS1) or an alternative one close to the N terminus (PTS2), the protein content of peroxisomes varies drastically. Here we suggest a new class of peroxisomes involved in microtubule (MT) formation. Eukaryotic cells assemble MTs from distinct points in the cell. In the fungus *Aspergillus nidulans*, septum-associated microtubule-organizing centers (sMTOCs) are very active in addition to the spindle pole bodies (SPBs). Previously, we identified a novel MTOC-associated protein, ApsB (*Schizosaccharomyces pombe* mto1), whose absence affected MT formation from sMTOCs more than from SPBs, suggesting that the two protein complexes are organized differently. We show here that sMTOCs share at least two further components, gamma-tubulin and GcpC (*S. pombe* Alp6) with SPBs and found that ApsB interacts with gamma-tubulin. In addition, we discovered that ApsB interacts with the Woronin body protein HexA and is targeted to a subclass of peroxisomes via a PTS2 peroxisomal targeting sequence. The PTS2 motif was necessary for function but could be replaced with a PTS1 motif at the C terminus of ApsB. These results suggest a novel function for a subclass of peroxisomes in cytoskeletal organization.

Peroxisomes are ubiquitous organelles of eukaryotes which are surrounded by a single membrane (9, 30). They serve a variety of functions, depending on the species, the cell type, and the environmental or developmental conditions. In mammals, peroxisomes are involved in a number of catabolic and anabolic pathways, most importantly, peroxide metabolism, the β-oxidation of long-chain fatty acids, and the biosynthesis of ether phospholipids (17, 37). The vital importance of the organelle in humans is shown by the existence of a number of severe and often lethal disorders that occur when the biogenesis of the organelle is impaired (36). In plants, peroxisomes are involved in photorespiration and typically contain the glyoxylate cycle, as in protozoa and yeast (8).

Given the complexity of peroxisomal functions, it is obvious that a large number of proteins need to be targeted to these organelles. Peroxisomal membrane and matrix proteins are synthesized on free ribosomes in the cytosol and are imported posttranslationally into preexisting organelles (9). The apparatus of protein import is clearly distinct from the import machinery of other organelles because it translocates folded and even oligomeric proteins and there is evidence that they are descending from the endoplasmic reticulum (6). A large number of peroxisomal proteins employ a tripeptide sequence at the C terminus, PTS1 (S/A/C-K/R/H-L/M) (7). A second class of proteins uses a sequence close to the N terminus which is less conserved, consists of R/K-L/I/V-X_5-H/Q-L/A, and is called PTS2 (33). In both cases, complex protein machineries are employed and some of the components appear to be used in PTS1- and PTS2-dependent protein translocation (9).

A very distinct class of peroxisomes is represented by the fungal Woronin body. This structure is named after a Russian mycologist who reported the characteristics of a distinct type of organelle in the fungus *Ascobolus pulcherrimus* (1, 39). Woronin bodies have been described in more than 50 species of ascomycota and deuteromycota but are missing in single-cell yeasts such as *Saccharomyces cerevisiae* and *Schizosaccharomyces pombe*. Thus, their function appears to be important for the filamentous life style. In *Neurospora crassa*, they appear as hexagonal bodies in the cell and upon cell damage plug the septal pores after a few seconds (15). This sealing mechanism is very important in syncytial organisms to prevent loss of the entire cytoplasm and hence death of the entire mycelium after one hypha is damaged (20). Their exact composition, however, remained obscure for many decades until G. Jedd and N.-H. Chua purified the organelle from *N. crassa* and identified the main constituent as a single protein named Hex1 (15, 42), because it forms hexagonal crystals. The existence of a PTS1 peroxisomal targeting sequence at the C terminus of the protein indicated that the Woronin bodies represent specialized peroxisomes. Hex1 displays some sequence similarity to eIF5, and it is thought that Hex1 derived from eIF5 during evolution

* Corresponding author. Mailing address: Karlsruhe Institute of Technology, Institute for Applied Biosciences, Department of Microbiology, Hertzstrasse 16, D-76187 Karlsruhe, Germany. Phone: 49-721-608-4630. Fax: 49-721-608-4509. E-mail: reinhard.fischer@KIT.edu.

† Present address: Technologie-Lizenz-Büro (TLB) der Baden-Württembergischen Hochschulen GmbH, Ettlinger Str. 25, D-76137 Karlsruhe, Germany.

‡ Equal contribution.

▽ Published ahead of print on 26 March 2010.

by gene duplication and subsequent modification of its function (42). Another example of a peroxisome-associated function may be the Pro40 protein in *Sordaria macrospora* (5). This protein is implicated in the regulation of sexual development.

In addition to the Woronin body close to the septal pore (22), we had evidence in *Aspergillus nidulans* that microtubule (MT) polymerization is initiated at septa. Using an MT plus-end-associated protein, the kinesin motor KipA (kinesin-7), we showed that the cytoplasmic area close to septa acts as an active MT-organizing center (MTOC) (16). Furthermore, we identified a novel MTOC-associated protein, ApsB, and localized it to the spindle pole bodies (SPBs) and to septa (35). The presence of septal MTOCs is similar to that in *S. pombe*, but there is no evidence for such organelles in the *S. cerevisiae*-related filamentous fungus *Ashbya gossypii* (18, 19). Given that MTOCs are generally composed of a large protein complex with gamma-tubulin as one characteristic member, we anticipate that MT polymerization at septa also requires a protein complex (40). Here we show for the first time the presence of gamma-tubulin at septal MTOCs (sMTOCs) and that it physically interacts with ApsB. Surprisingly, ApsB is associated with a subclass of peroxisomes in the cytoplasm, and we propose that they are involved in septal MTOC formation.

MATERIALS AND METHODS

Strains, plasmids, and culture conditions. The preparation of the supplemented minimal and complete media used for *A. nidulans* and the standard strain construction procedures used are described in reference 11. To isolate total DNA and RNA, corresponding strains were grown in liquid culture for 16 h. Mycelium was harvested and immediately processed for total DNA (see below). A list of the *A. nidulans* strains used in this study is given in Table 1. Standard laboratory *Escherichia coli* strains (XL-1 blue and Top10) were used. The plasmids used are listed in Table 2.

Light and fluorescence microscopy. For live-cell imaging, cells were grown in glass-bottom dishes (FD35-100; World Precision Instruments, Berlin, Germany) in 2 ml of minimal medium (MM) containing either 2% glycerol or 2% glucose as a carbon source. Medium was supplemented with pyridoxine, *p*-aminobenzoic acid, biotin, arginine, uracil, or uridine, depending on the auxotrophy of the strains. Cells were incubated at room temperature for 1 to 2 days, and images were captured using an Axiophot microscope (Zeiss, Jena, Germany), a Plan-apochromatic 63× or 100× oil immersion objective lens, and an HBO50 Hg lamp. Alternatively, a Zeiss AxioImager Z1 with AxioVision software (V4.5) was used. Fluorescence was observed using standard Zeiss filter combinations no. 09 (fluorescein isothiocyanate, green fluorescent protein [GFP]) and no. 15 (monomeric red fluorescent protein 1 [mRFP1], DsRed). Laser images were obtained using the Zeiss Cell Observer SD, which combines the high-end Cell Observer microscopy platform and the CSU-X1 spinning-disc technology from Yokogawa for high-speed confocal microscopy. Images were collected and analyzed with a Hamamatsu Orca ER II camera system and the Wasabi software (version 1.2) or a Zeiss Axiocam and AxioVision software. Image and video processing was done with the Wasabi software from Hamamatsu, Adobe Photoshop, ImageJ (NIH, Bethesda, MD), and virtual dub (http://www.virtualdub.org).

Molecular techniques. Standard DNA transformation procedures were used for *A. nidulans* (41) and *E. coli* (27). For PCR experiments, standard protocols were applied using a Biometra Personal Cycler (Biometra, Göttingen, Germany) for the reaction cycles. DNA sequencing was done commercially (MWG Biotech, Ebersberg, Germany). Total DNA was extracted from *A. nidulans* in the following way. Spores were inoculated into liquid MM plus supplements and grown for 12 to 18 h at 30°C without shaking. Hyphal mats were harvested, dried with tissue paper, and ground in liquid nitrogen. The resulting powder was mixed with extraction buffer (50 mM EDTA, 0.2% sodium dodecyl sulfate [SDS]) and incubated for 30 min to 2 h at 68°C in a water bath. SDS and proteins were removed from the suspension by addition of potassium-acetate solution (8 M, pH 4.2) and centrifugation. Total DNA was precipitated from the supernatant with isopropanol, and the pellet was washed twice with 70% ethanol, air dried, resuspended in TE buffer with RNase A, and stored at 4°C. Southern hybridizations were performed according to the DIG Application Manual for Filter Hybridization (Roche Applied Science, Technical Resources, Roche Diagnostics GmbH, Mannheim, Germany).

Bimolecular fluorescence complementation assay (BiFC). The enhanced yellow fluorescent protein (eYFP)-tagged N-terminal half (YFP^N) was amplified using primers 5′-C*GGTACC*ATGGTGAGCAAGGGCGAGGAGCTG-3′ (fwd_Kpn_YFP-N) and 5′-C*GGCGCGCCC*CGTGGCGATGGAGCGCATGATATAGACGTTGTGGCTGTTGTAG-3′. For the C-terminally eYFP-tagged (YFP^C) half, primers 5′-C*GGTACC*ATGGCCGACAAGCAGAAGAACGGCATCAAGG-3′ (fwd_Kpn_YFP-C) and 5′-C*GGCGCGCC*GTGGTTCATGACCTTCTGTTTCAGGTCGTTCGGGATCTTGCAGGCCGGGCGCTTGTACAGCTCGTCCATGCCGAGAGTGATCCC-3′ (rev_YFP-C_Li_Asc) were used. These primers introduced KpnI and AscI restriction sites (in italics) in addition to the protein linker sequences RSIAT (YFP^N) and RPACKIPNDLKQKVMNH (YFP^C) (underlined). eYFP was split at bp 460 to 462 by using the ATG codon as the start of the YFP^C half. PCR fragments were subcloned into pCR2.1-Topo (Invitrogen, Karlsruhe, Germany), subsequently released with KpnI and AscI, and used to replace GFP2-5 of pMCB17apx-apsB (35), giving pDV7 (YFP^N) and pDV8 (YFP^C). Full-length $apsB^{3.2}$ (3.2 kb) was taken from pDV21a and cloned into pDV7, giving pDV22b [$alcA(p)::YFP^N::apsB^{3.2}$], and full-length $\gamma tubulin^{1.8}$ was amplified using primers 5′-C*GGCGCGCCC*CGGGATGCCTAGGTATACCCTC-3′ (Gamma_tub_Asc_fwd) and 5′-C*TTAATTAA*TTATACTCCAACTTCATCCTTTCC-3′ (Gamma_tub_Pac_rev) (the AscI and PacI restriction sites are in italics, and the start and stop codons are underlined) and cloned into pDV8, giving pDV50 [$alcA(p)::YFP^C::\gamma tubulin^{1.8}$]. For BiFC analysis, pDV22 and pDV50 were combined and transformed into GR5, giving SNZ11. The cloned gene length is indicated as exponents; e.g., the length of the cloned gene $apsB^{3.2}$ is 3.2 kb. Similarly, *hexA* was amplified using primers 5′-C*GGCGCGCCC*CGGGATGGGTTACTACGACGACG-3′ (hexA_Asc_fwd) and 5′-C*TTAATTAA*TTATAGACGGGAAGAGTGGATGATC-3′ (hexA_Pac_rev1; 680 bp to stop codon) or 5′-G*TTAATTAA*CCTCAATCAAGTGCAAGGTTTCG-3′ [hexA_Pac_rev2; 1 kb, including the poly(A) site] and cloned into pDV8, giving pDV17 [$alcA(p)::YFP^C::hexA^{680}$], and into pDV7, giving pDV19a [$alcA(p)::YFP^N::hexA^{1.0}$]. For BiFC analysis, pDV17 and pDV22b were combined and transformed into GR5, giving SDV42, or pDV19a and pDV23a were combined, giving SDV43.

Protein extracts, immunoprecipitation, and Western blotting. To prepare protein extracts, *A. nidulans* strains SNZ-SI 42 [$alcA(p)::3\times HA::apsB^{3.2}$], SNZ16 [$alcA(p)::GFP::\gamma tubulin^{1.8}$], and SNZ37 [$alcA(p)::apsB^{3.2}::3\times HA$ $alcA(p)::GFP::\gamma tubulin^{1.8}$] were incubated in liquid MM for 24 h at 37°C. The medium was supplemented with 0.2% glucose and 2% threonine to induce the *alcA* promoter. The mycelium was harvested by filtration through Miracloth (Calbiochem, Heidelberg, Germany), dried between paper towels, and immediately ground in liquid nitrogen. Afterwards, the mycelial powder was resuspended in protein extraction buffer (20 mM Tris-HCl, pH 8, 150 mM NaCl, 0.01% Triton X-100) containing protease inhibitor (2 mM phenylmethylsulfonyl fluoride [PMSF]) and vortexed for 5 min at 4°C. Cell debris was pelleted by two centrifugations (Eppendorf centrifuge 5403; Eppendorf, Hamburg, Germany) at 13,000 rpm at 4°C for 10 min. A volume of 1 ml protein extract was adjusted to 300 mM NaCl and incubated with monoclonal antibody HA.11 (dilution, 1:200; clone 16B12; Hiss Diagnostics, Freiburg, Germany). After 1 h of incubation at 4°C, 50 μl protein-G-agarose (Roche, Mannheim, Germany) was added and the mixture was incubated for an additional 3 h. Agarose beads were pelleted by centrifugation in an Eppendorf centrifuge at 15,000 rpm at 4°C for 30 s and washed three times with 1 ml extraction buffer containing protease inhibitor (2 mM PMSF) with different NaCl molarities (150 mM NaCl, 500 mM NaCl, and no NaCl). After the denaturation of the samples, protein extracts and coimmunoprecipitated pellets were loaded onto an 8% SDS-polyacrylamide gel. For Western blotting, a polyclonal antibody raised against GFP (product G1544; dilution, 1:4,000; Sigma-Aldrich, Munich, Germany) with anti-rabbit IgG peroxidase conjugate secondary antibody (product A0545; dilution, 1:4,000; Sigma-Aldrich, Munich, Germany) in the case of gamma-tubulin and the anti-HA antibody (clone 16B12; dilution, 1:1,000) with anti-mouse IgG peroxidase conjugate secondary antibody (product A2304; dilution, 1:10,000; Sigma-Aldrich, Munich, Germany) in the case of ApsB were used. Nitrocellulose membranes used for blotting were from Schleicher & Schuell (Dassel, Germany).

Yeast two-hybrid screen. A full-length cDNA fragment of *apsB* was amplified with primers 5′-*GGATCC*GAATGACTCTAAAAGAGC-3′ and 5′-*GTCGAC*TCAAACTTCGATATCAAC-3′ and cloned into the BamHI-SalI restriction sites of pGBT9 (Clontech), giving pRS89, and into pGAD424 (Clontech), giving pRS88. A cDNA fragment from a cDNA library containing the full-length *hexA* gene was cloned into of the yeast GAL4-Matchmaker system (Clontech), giving pRS91. Transformation of yeast strains, selection for diploids, a histidine growth assay, and a β-galactosidase (β-Gal) assay were done as described in reference 2.

TABLE 1. *A. nidulans*, *E. coli*, and *S. cerevisiae* strains used in this study

Strain	Genotype	Source
AJC1.5	*biA1 apsB6*	J. Clutterbuck (1969)
AJC1.7	*biA1 apsB10*	J. Clutterbuck (1969)
FGSC89	*biA1 argB2*	FGSC
GJA28	*biA1* Δ*hexA*::*argB* (FGSC89 transformed with Δ*hexA*::*argB* deletion cassette)	G. Jedd, Singapore
GR5	*pyrG89 wA3 pyroA4*	38
MH11269	*biA1 niiA4 pyroA4 pexC*::*bar*	12
SDV38	*alcA*(*p*)::*GFP*::*hexA*^{680} *wA3 pyroA4* (GR5 transformed with pDV15)	This work
SDV42	*alcA*(*p*)::*YFP*^{N}::*apsB*$^{3.2}$ *alcA*(*p*)::*YFP*^{C}::*hexA*^{680} *wA3 pyroA4* (GR5 transformed with pDV17 and pDV22b)	This work
SDV43	*alcA*(*p*)::*YFP*^{N}::*hexA*$^{1.0}$ *alcA*(*p*)::*YFP*^{C}::*apsB*$^{3.2}$ *wA3 pyroA4* (GR5 transformed with pDV19a and pDV23a)	This work
SDV49-4	*alcA*(*p*)::*mRFP1*::*apsB*$^{1.5}$ *alcA*(*p*)::*GFP*::*hexA*^{680} *pyroA4* Δ*nkuA*::*argB* (TN02A3 transformed with pDV15 and pDM8a)	This work
SDV70b	*yA1 pyroA4 riboB2 areA102 gpd*(*p*)::*GFP*::*acuE alcA*(*p*)::*mRFP1*::*apsB* (TALX207-10 transformed with pDV42a)	This work
SDV73	*alcA*(*p*)::*GFP*::*apsB*$^{1.5}$ *alcA*(*p*)::*mRFP1*::*hexA*^{680} *pyroA4* Δ*nkuA*::*argB* [TN02A3 transformed with pDV39 and pMCB17apx(-apsB)]	This work
SDV77	*alcA*(*p*)::*GFP*::*apsB-PTS2.1 pyroA4* Δ*nkuA*::*argB* (TN02A3 transformed with pDV43)	This work
SDV78c	*alcA*(*p*)::*mRFP1*::*hexA*^{680} *gpd*(*p*)::*GFP*::*acuE yA1 riboB2 areA102* (TALX207-10 transformed with pDV39 and pTN1)	This work
SDV79	Δ*hexA alcA*(*p*)::*GFP*::*apsB_PTS2*^{mut} (GJA28 crossed with SDV77a)	This work
SDV80	*apsB6 alcA*(*p*)::*GFP*::*apsB_PTS2*^{mut} (AJC1.5 crossed with SDV77)	This work
SDV88	*apsB6 alcA*(*p*)::*GFP*::*apsB*$^{1.5}$ (AJC1.5 crossed with SEa3)	This work
SDV95	Δ*hexA* Δ*apsB alcA*(*p*)::*GFP*::*apsB_PTS2*^{mut} (SDV82 crossed with SRS25)	This work
SDV98	*apsB10 alcA*(*p*)::*GFP*::*tubA* (AJC1.7 crossed with SJW02)	This work
SDV103	*apsB10 alcA*(*p*)::*GFP*::*tubA alcA*(*p*)::*GFP*::*apsB_PTS2*^{mut} (SDV98 transformed with pDV43a)	This work
SEa3	*alcA*(*p*)::*GFP*::*apsB wA3 pyroA4*	35
SJW02	*alcA*(*p*)::*GFP*::*tubA* Δ*argB*::*trpC*Δ*B wA3 pyroA4*	35
SNZ11	*alcA*(*p*)::*YFP*^{N}::*apsB*$^{3.2}$ *alcA*(*p*)::*YFP*^{C}::γ*tubulin*$^{1.8}$ *wA3 pyroA4* (GR5 transformed with pDV22 and pDV50)	This work
SNZ16	*alcA*(*p*)::*GFP*::γ*tubulin*$^{1.8}$ *pyroA4* (TN02A3 transformed with pNZ17)	This work
SNZ22	*alcA*(*p*)::*GFP*::γ*tubulin*$^{1.8}$ *gpd*(*p*)::*DsRed*::*stuA*(*NLS*) (SNZ16 transformed with pJH19 and pTN1)	This work
SNZ34	*apsB10 alcA*(*p*)::*GFP*::*apsB_PTS2*^{mut}*_SRL* (AJC1.7 transformed with pNZ16)	This work
SNZ37	*alcA*(*p*)::*GFP*::γ*tubulin apsB*::3×*HA* (SNZ16 transformed with pNZS23 and pTN1)	This work
SNZ59	*apsB*(*p*)::*GFP*::*apsB pyroA4* (TN02A3 transformed with pNZ-SI37)	This work
SNZ61	γ*tubulin*(*p*)::*GFP*::γ*tubulin pyroA4* (TN02A3 transformed with pNZ-SI36)	This work
SNZ94	*pabaA1 biA1 alcA*(*p*)::*GFP*::*apsB_PTS2*^{mut}*_SRL gpd*(*p*)::*GFP*:*stuA*(*NLS*) Δ*apsB*::*argB trpC801* (SRS24 transformed with pNZ16)	This work
SNZ-SH80	*alpB*(*p*)::*alpB*::*GFP pyroA4* Δ*nkuA*::*argB* (SO451 transformed with *alpB*::GFP::*pyrG*::RB-*alpB* fusion PCR)	This work
SNZ-SI 42	*alcA*(*p*)::3×*HA*::*apsB pyroA4* (TN02A3 transformed with pSI-N4)	This work
SO451	*pyrG89 wA3 pyroA4* Δ*nkuA*::*argB*	FGSC
SRS24	*gpd*(*p*)::*GFP*::*stuA*(*NLS*) *pabaA1* Δ*apsB*::*argB trpC801*	31
TALX207-10	*yA1 pyroA4 areA102* transformed with *gpd*(*p*)::*GFP*::*acuE* and *riboB*+ plasmid	M. Hynes and A. Andrianopoulos, Melbourne, Australia
TNO2A3	*pyrG89 pyroA4* Δ*nkuA*::*argB*	S. Osmani
PJ69-4A	*MAT***a** *trp1-901 leu2-3 ura3-52 his3-200 gal4*Δ *gal80*Δ *GAL2-ADE-LYS*::*GAL1-HIS3 met2*::*GAL7-lacZ*	2
AH109	*MAT***a** *trp1-901 leu2-3,112 ura3-52 his3-200 gal4*Δ *gal80*Δ *LYS2*::*GAL1UAS-GAL1TATA-HIS3 GAL2UAS-GAL2TATA-ADE2 URA3*::*MEL1UAS-MEL1TATA-lacZ GAL2-ADE-LYS*::*GAL1-HIS3 met2*::*GAL7-lacZ*	13
Y187	*MAT*α *ura3-52 his3-200 ade2-101 trp1-901 leu2-3,112 gal4*Δ *met-gal80*Δ *URA3*::*GAL1UAS-GAL1TATA-lacZ*	P. Uetz, Karlsruhe, Germany

[a] FGSC, Fungal Genetics Stock Center.

The yeast strains used for transformation were AH109, Y187, and PJ69-4A (Clontech).

Site-directed mutagenesis. The peroxisomal target sequence of *apsB* was mutated using pDV21a as the template and the QuikChange XL site-directed mutagenesis kit from Stratagene. The last two amino acids were mutated using primer 5′-GCGATTTGGAGAAGCTACGTAAGACCAGCAGTCAGATAAGGAG-3′ and the corresponding antiparallel primer, giving pDV43. Successful mutagenesis was confirmed by commercial sequencing (MWG Biotech, Ebersberg, Germany).

GFP or mRFP1 tagging of proteins. pMCB17apx was used as the basic vector for the tagging of *apsB* or *hexA* with GFP, and pDM8 was used for tagging with mRFP1 (see reference 35). Full-length *hexA* was amplified from genomic DNA using primers 5′-*CGGCGCGCCC*GGGATGGGTTACTACGACGACG-3′ and 5′-*CTTAATTAA*TTATAGACGGGAAGAGTGGATGATC-3′.

To obtain *in vivo* protein expression levels, we expressed the proteins under the control of the corresponding natural promoters. The *apsB* promoter (1.33 kb) was amplified from genomic DNA using primers 5′-*GCCTAGG*CAAGCCGCAACTCCC-3′ (apsB_nat(p)_AvrII_fwd) and 5′-*CGGTACC*GGATCTG

TABLE 2. Plasmids used in this study

Plasmid	Construction	Source
pCR2.1-TOPO	Cloning vector	Invitrogen
pDM8a	GFP replaced with mRFP1 in pMCB17apx-apsB	35
pDV7	*alcA*(*p*)::*YFP*^{N}::*apsB*$^{1.5}$ *pyr4* GFP of pMCB17apx-apsB replaced with *YFP*^{N}	This work
pDV8	*alcA*(*p*)::*YFP*^{C}::*apsB*$^{1.5}$ *pyr4* GFP of pMCB17apx-apsB replaced with *YFP*^{C}	This work
pDV15	*alcA*(*p*)::*GFP*::*hexA*^{680} *pyr4* pMCB17apx with full-length *hexA*	This work
pDV17	*alcA*(*p*)::*YFP*^{C}::*hexA*^{680} *pyr4 apsB* of pDV8 replaced with *hexA*^{680}	This work
pDV19	*alcA*(*p*)::*YFP*^{N}::*hexA*$^{1.0}$ *pyr4 apsB* of pDV7 replaced with full-length *hexA*$^{1.0}$	This work
pDV21a	pMCB17-apx containing full-length *apsB* of 3.2 kb between AscI and PacI restriction sites; *alcA*(*p*)::*GFP*::*apsB*$^{3.2}$ *pyr4*	This work; 35
pDV22b	*alcA*(*p*)::*YFP*^{N}::*apsB*$^{3.2}$ *pyr4 apsB* of pDV7 replaced with full-length *apsB*$^{3.2}$	This work
pDV23	*alcA*(*p*)::*YFP*^{C}::*apsB*$^{3.2}$ *pyr4 apsB* of pDV8 replaced with full-length *apsB*$^{3.2}$	This work
pDV39	*alcA*(*p*)::*mRFP1*::*hexA*^{680} *pyr4 apsB of* pDM8a changed with *hexA*^{680}	35
pDV42a	*alcA*(*p*)::*mRFP*::*apsB*$^{3.2}$ *pyr4* pDM8a with full-length *apsB*$^{3.2}$	35
pDV43	PTS2 of *apsB* in pDV21a is mutated *alcA*(*p*)::*GFP*::*apsB_PTS2*^{mut} *pyr4*	This work
pDV50	*alcA*(*p*)::*YFP*^{C}::*γtubulin*$^{1.8}$ *pyr4 apsB* of pDV8 replaced with full-length *γtubulin*$^{1.8}$	This work
pENTR^{MT}/D-Topo	Cloning vector	Invitrogen
pJH19	*gpd*(*p*)::*stuA*(*NLS*)::*DsRed argB*	34
pMCB17apx(-apsB)	pMCB17 version for fusion of GFP to N termini of proteins of interest (with 1.5 kb of *apsB*)	35; V. P. Efimov
pMT-3 × HA	Gateway destination vector	34
pNZ16	*PTS1* (*SRL*) added before stop codon of *apsB_PTS2*^{mut} in pDV43; *alcA*(*p*)::*GFP*::*apsB_PTS2*^{mut}*_SRL pyr4*	This work
pNZ17	pMCB17-apx containing full-length *γtubulin* of 1.8 kb between AscI and PacI restriction sites; *alcA*(*p*)::*GFP*::*γtubulin*$^{1.8}$ *pyr4*	This work
pNZ21	*apsB*$^{3.2}$ without stop codon in pENTR^{MT}/D-Topo	
pNZS23	*apsB*$^{3.2}$ from pNZ21 cloned into pMT-3 × HA *alcA*(*p*)::*apsB*$^{3.2}$::3 × *HA argB*	This work
pNZ-SI36	*alcA*(*p*) of pNZ17 replaced with 1.16-kb *γtubulin*(*p*) EcoRI and BsiwI restriction sites; *γtubulin*(*p*)::*GFP*::*γtubulin*$^{1.8}$ *pyr4*	This work
pNZ-SI37	*alcA*(*p*) of pDV21 Replaced with 1.33-kb *apsB*(*p*) AvrII and KpnI restriction sites; *apsB*(*p*)::*GFP*::*apsB*$^{3.2}$ *pyr4*	This work
pRS88	*apsB* in BamHI-SalI sites of pGAD424	This work
pRS89	*apsB* in BamHI-SalI sites of pGBT9	This work
pRS91	cDNA clone of *hexA* in pGAD424	This work
pSI-N4	pSM14 containing full-length *apsB* of 3.2 kb between AscI and PacI restriction sites; *alcA*(*p*)::3×*HA*::*apsB*$^{3.2}$ *pyr4*	This work
pSM14	*GFP* of pMCB17apx replaced with 3×*HA* between KpnI and AscI restriction sites	25
pTN1	*pyroA* from *A. fumigatus*	23

CCACTGCG-3′ (apsB_nat(p)_KpnI_rev) (the AvrII and KpnI restriction sites are in italics), cloned instead of *alcA*(*p*) into pDV21, giving pNZ-SI37 [*apsB*(*p*)::*GFP*::*apsB*], and transformed into TN02A3, giving SNZ59. The gamma-tubulin promoter (1.16 kb) was amplified from genomic DNA using primers 5′-*GGAATTC*CATACCCAGCATAAATTCGG-3′ (Gamma_tub_nat(p)_EcoRI_fwd) and 5′-*CCGTACG*CTTTCTTGCTTGCCTTAAG-3′ (Gamma_tub_nat(p)_BsiwI_rev) (EcoRI and BsiwI restriction sites are in italics), cloned instead of *alcA*(*p*) into pNZ17, giving pNZ-SI36 (*γtubulin*(*p*)::*GFP*::*γtubulin*$^{1.8}$), and transformed into TN02A3, giving SNZ61. AlpB AN4867 (*S. pombe* Alp6) was amplified via fusion PCR using primers 5′-GGGAGGACAAATACAAACTCG-3′ (Alp6_mitte_fwd) and 5′-ctccagcgcctgcaccagctccTTGCTCAGTCGAATCCTTC TTTTC-3′ (Alp6_linker_rev) to amplify the C-terminal fragment of AlpB without the stop codon and primers 5′-atcagtgcctcctctcagacagTAGCATACATGCA GTACATTTCTCG-3′ (Alp6_RB_link_fwd) (linkers in lower case letters) and 5′-ACCGTCATGGCAGAAACGAAG-3′ (Alp6_RB_rev) to amplify the right border of AlpB. The two PCR products were fused to a *GFP-pyrG* PCR cassette (kindly provided by S. Osmani, Ohio State University) to generate a 5.5 fusion PCR product using primers 5′-CCAGTCTCGAGACCTCAATT G-3′ (Alp6_Nprimer_fwd) and 5′-TTATCACCTGCTGGTTCTGAG-3′ (Alp6_Nprimer_rev). The fusion PCR product was transformed into *A. nidulans* strain SO451, giving SNZ-SH80 [*alpB*(*p*)::*alpB*::*GFP*].

Generation of the *apsB*$^{3.2}$*_PTS2*^{mut}*_SRL* (PTS1) construct. A PTS1 targeting sequence (SRL) was added to the C terminus of ApsB by amplifying the full-length mutated gene *apsB*$^{3.2}$*_PTS2*^{mut} in pDV43 using primers 5′-TTTG *GGCGCGCCC*CGGCATGACTCTAAAAGAGCAAAGTAGTACG-3′ (apsB_Asc_fwd) and 5′-CC*TTAATTAA*TCAtagacgggaAACTTCGATATC-3′ (SRL_PTS1_PacI_rev) (PTS1 is in lowercase letters). The PCR product was cloned between the AscI and PacI restriction sites in the vector pMCB17apx and confirmed via sequencing, giving plasmid pNZ16, which was transformed into *apsB10* mutant strain AJC1.7, generating strain SNZ34 [*apsB10*, *alcA*(*p*)::*GFP*::*apsB_PTS2*^{mut}*_SRL*]. Ectopic integration of the construct and the presence of the mutated endogenous *apsB* locus were confirmed by PCR, Southern blotting, and sequencing of the PCR products. Likewise, transformation of the *apsB* construct was done with pNZ16 into *apsB* deletion strain SRS24, generating SNZ94 with the same rescue phenotype as in the case of AJC1.7.

Immunostaining. Spores (10^3/ml) were inoculated with 0.5 ml MM on sterile coverslips for 12 to 24 h at room temperature (RT). Cells were fixed for 30 min with formaldehyde and digested for 1 h using digestion solution (Glucanex, β-D-glucanase, lyticase, and Driselase in Na-phosphate buffer with 50% egg white), washed with PBS, incubated in −20°C methanol for 10 min, and blocked with Tris-buffered saline–Tween 20 (TBST) plus 5% skim milk before incubation with the first monoclonal antibody (anti-gamma-tubulin T6657 at 1:500; Sigma-Aldrich) in TBST overnight at 4°C. Next, cells were washed and incubated with the Alexa Fluor^{546}-labeled goat anti-mouse secondary antibody (A11003 at 1:200 in TBST; Molecular Probes) for 1 h at RT. Cells were washed and mounted on microscope slides (with VECTASHIELD mounting medium with DAPI [4′,6-diamidino-2-phenylindole]), sealed with nail polish, and stored at 4°C overnight in the dark before microscopy.

RESULTS

Identification of gamma-tubulin and GcpC^{Alp6} at septal MTOCs and interaction of ApsB with gamma-tubulin. *A. nidulans* ApsB has been localized at SPBs and at septa, suggesting the presence of MTOCs at septa (Fig. 1) (35). MTOCs are large protein complexes which consist of several proteins, gamma-tubulin, and associated gamma-tubulin complex proteins, which are mostly conserved from yeast to humans (26). Un-

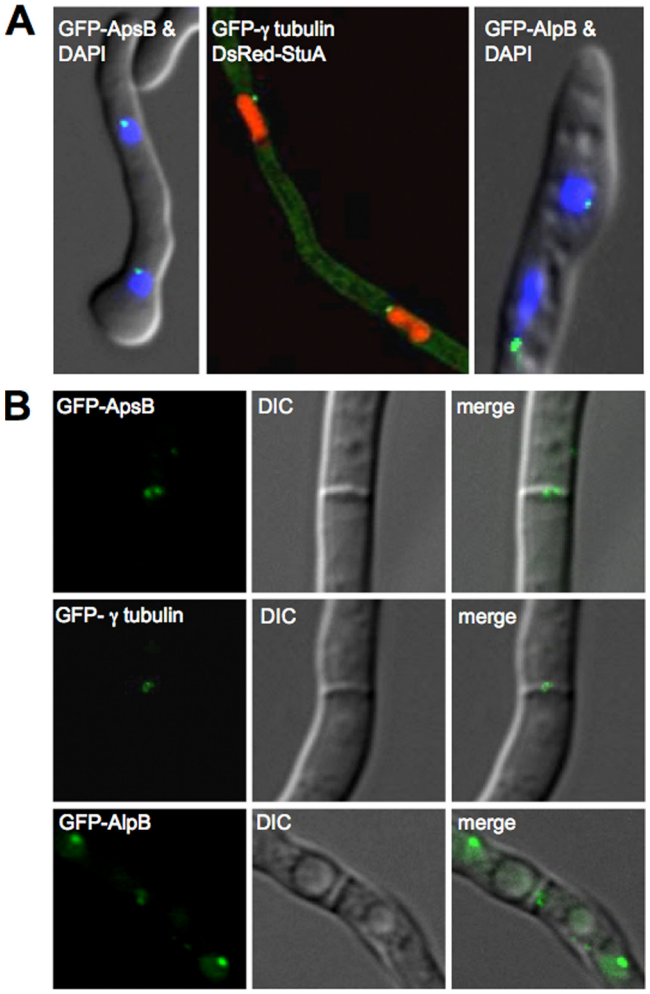

FIG. 1. Gamma-tubulin and AlpB localize to septal MTOCs. (A) GFP-ApsB, GFP–gamma-tubulin, and $AlpB^{Alp6}$-GFP localize to the SPBs. Nuclei are stained with DsRed-StuA(NLS) (SNZ22) or DAPI. (B) Localization of the same GFP-tagged proteins to the septal pore (two spots in the center). Fluorescence (left), differential interference contrast (DIC, middle), and merged (right) microscopic images are shown. The strains used were SNZ59 (GFP-ApsB), SNZ61 (GFP–gamma-tubulin), and SNZ-SH80 ($AlpB^{Alp6}$-GFP). All proteins were expressed from their natural promoters.

fortunately, the most important protein of MTOCs, gamma-tubulin, has not been identified at septa of *A. nidulans* before. In our own experiments, we were able to detect a very weak signal at septa when gamma-tubulin was expressed from its own promoter and fused to GFP. In *S. pombe*, it has also been reported that gamma-tubulin was present at nonnuclear MTOCs in very small amounts and thus was also not easy to detect (29). To further elucidate the composition of septal MTOCs, we searched the *A. nidulans* genome for a homologue of *S. pombe* Alp6 (*S. cerevisiae* Spc98, human Gcp3) and identified the open reading frame AN4867 (968 amino acids in length) with 35% identity to Alp6. In order to localize the corresponding protein, we constructed a C-terminal GFP fusion protein expressed from the native promoter and transformed it into *A. nidulans* (SO451). The protein localized to MTOCs at nuclei and at septa, indicating that the two MTOCs also share this protein (Fig. 1). During the course of our experiments, this gene was analyzed in the laboratory of B. Oakley and was named *gcpC* (40).

In order to demonstrate that ApsB and gamma-tubulin colocalize at MTOCs, we visualized gamma-tubulin in a GFP-ApsB-expressing strain (Fig. 2A). Next, we showed that ApsB not only colocalizes but also interacts with gamma-tubulin. To this end, we applied the BiFC assay system and fused full-length ApsB with the N-terminal part of YFP and full-length gamma-tubulin with the C-terminal part of YFP. Corresponding *A. nidulans* strains showed a YFP signal at nuclei and at septa (Fig. 2B). Interestingly, we also found a fluorescence signal at the tips of all actively growing hyphae (Fig. 2C). Previously, ApsB had already been found at the hyphal tip and growing MTs were also reported to originate from the hyphal tip in some cases (16, 35). Gamma-tubulin alone was not visible at the hyphal tip, probably due to the high cytoplasmic background. Some cytoplasmic spots were also observed, as shown before for ApsB alone (35). Control experiments with ApsB or gamma-tubulin alone did not result in any fluorescence.

The ApsB–gamma-tubulin interaction result was confirmed by coimmunoprecipitation using hemagglutinin (HA)-ApsB and GFP–gamma-tubulin tagged proteins. Gamma-tubulin was detected in the precipitate obtained with anti-HA antibodies (Fig. 2D).

ApsB is associated with peroxisomes. To further analyze the role of ApsB, we employed a yeast two-hybrid analysis. The cDNA of *apsB* was cloned into pGBT9 (pRS89) and transformed into PJ69-4A. This strain was used as a recipient strain for a yeast two-hybrid gene bank kindly provided by S. Osmani (24). Besides ApsB itself, we identified five putative interacting clones (three unknown proteins, one Zn^{2+} finger protein, and one putative nucleoside transporter). The translation product of one of the clones displayed sequence identity to *A. nidulans* HexA, the homologue of the *N. crassa* Hex-1 protein (15). To prove the interaction between ApsB and HexA, we cloned the full-length *hexA* gene and tested it in the interaction screen. A yeast strain of mating type **a** (AH109) containing the GAL4 binding domain with *apsB* (Y2HapsB-BD) was crossed to a yeast strain of mating type α (Y187) containing the GAL4 activation domain with *apsB* (Y2HapsB-AD), *hexA* (Y2HhexA-AD), or just the empty vector (pGAD424) as a control. Diploids were identified by selective growth on YEPD agar medium lacking leucine and tryptophan (YEPD LT^-) (Fig. 3A), as described by Cagney et al. (2). To look for positive protein-protein interactions, colonies were subsequently inoculated onto YEPD medium lacking leucine, tryptophan, and histidine (YEPD LTH^-) (Fig. 3B). This medium allows growth only if the strains produce their own histidine due to a positive interaction of the respective proteins. Colonies with *apsB*/*apsB* and *apsB*/*hexA* grew well in comparison to the *apsB*/empty-vector combination. The weak background growth was reduced by the addition of 3 mM 3-amino-1,2,4-triazole (3-AT) (Fig. 3C). The positive interaction was confirmed with the β-Gal assay on membranes. ApsB interacted with itself, as well as with HexA, while in combination with the empty vector no reaction occurred (Fig. 3D). To exclude the possibility that neither HexA nor ApsB has an intrinsic affinity for other proteins and gives false positives in the yeast two-hybrid assay, we tested both of

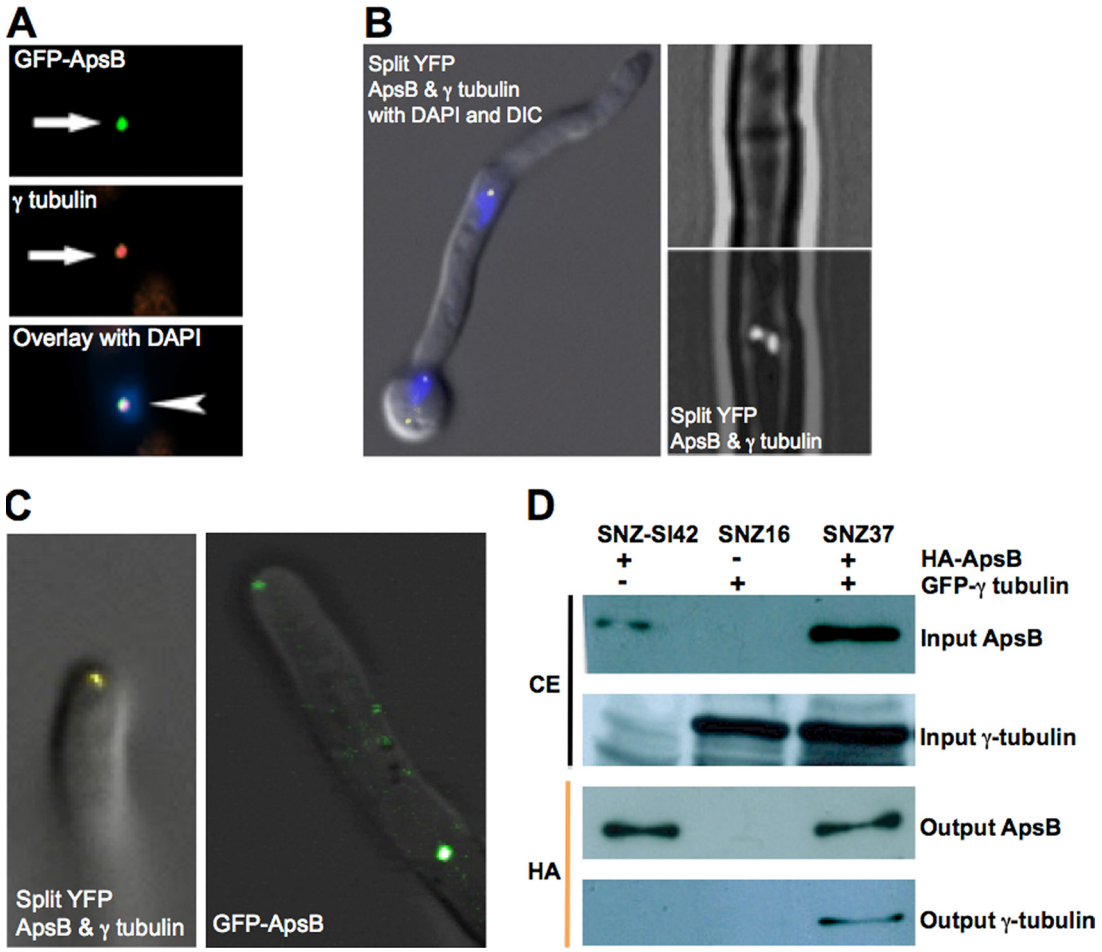

FIG. 2. Colocalization and interaction of ApsB with gamma-tubulin. (A) Colocalization of GFP-ApsB and gamma-tubulin using secondary immunofluorescence to detect gamma-tubulin with Alexa-Fluor^{546}-labeled secondary antibodies. (B) BiFC of ApsB and gamma-tubulin (SNZ11). Fluorescent signals, indicating an interaction between ApsB and gamma-tubulin, were found at the SPBs (left) and to the center of septal pores as two spots (right). The upper image is a differential interference contrast (DIC) picture, and the lower image is a fluorescent picture merged with the upper DIC picture. (C) Fluorescent signals of interacting ApsB with gamma-tubulin (BiFC) and of GFP-ApsB in the hyphal tip. (D) Confirmation of the ApsB–gamma-tubulin interaction by coimmunoprecipitation. SNZ37 [*alcA*(*p*)::*apsB*::3×*HA alcA*(*p*)::*GFP*::γ*tubulin*$^{1.8}$] was used for this assay, and SNZ-SI 42 [*alcA*(*p*)::3×*HA*::*apsB*$^{3.2}$] and SNZ16 [*alcA*(*p*)::*GFP*::γ*tubulin*$^{1.8}$] were the control strains. Anti-HA antibodies (clone 16B12 derived from a mouse; Hiss Diagnostics, Freiburg, Germany) were used for immunoprecipitation. Precipitation was performed in 1 ml crude extract (CE) of approximately 10 mg/ml total protein and 50 μl protein G-agarose (Roche, Mannheim, Germany). Western blot detection was done with anti-GFP antibodies (anti-GFP N terminus, derived from a rabbit, product G1544; Sigma-Aldrich, Munich, Germany) in the case of gamma-tubulin and with the anti-HA antibodies (clone 16B12) in the case of ApsB.

them and the empty vector against a library of *Treponema pallidum* with 73 different proteins (kindly provided by P. Uetz) (not shown). Growing on YPED LTH$^-$, the empty vector produced three strains (4%) with a false-positive reaction, which were also seen for *apsB* and *hexA*. Despite these, no positive interaction with any of the remaining 70 *T. pallidum* proteins was found, indicating that neither ApsB nor HexA interacts randomly with given proteins and confirming that the HexA/ApsB interaction was specific. Sequence inspection of ApsB revealed a putative peroxisomal targeting sequence (PTS2), KIRDLEKQL, at amino acid positions 66 to 74. Likewise, proteins with sequence similarity to ApsB (29), such as mto1 (formerly known as mod20 or mbo1) and pcp1 (*S. pombe*), NCU02332.1 and NCU02411.1 (*N. crassa*), and AAH46878 (*Drosophila melanogaster*) and CDK5RAP2 (*Homo sapiens*) all have a possible PTS2, as identified with the software program psort (http://psort.hgc.jp/).

ApsB localizes to a subclass of peroxisomes. To obtain further proof of the peroxisomal localization of ApsB, we compared its localization with the localization of the peroxisomal enzyme AcuE (acetate-malate synthase). This protein was tagged with GFP (strain TALX207-10, kindly provided by M. Hynes and A. Andrianopoulos, Melbourne, Australia) and coexpressed in a strain with mRFP1-ApsB (strain SDV70b). Fourteen percent of the spots showed green and red fluorescence (Fig. 4A). In addition, we analyzed GFP-AcuE and mRFP1-tagged HexA (SDV78c), which confirmed the localization of mRFP1-HexA to peroxisomes (Fig. 4B). However, one important difference between ApsB and HexA was the frequency of colocalization with AcuE. While HexA and AcuE

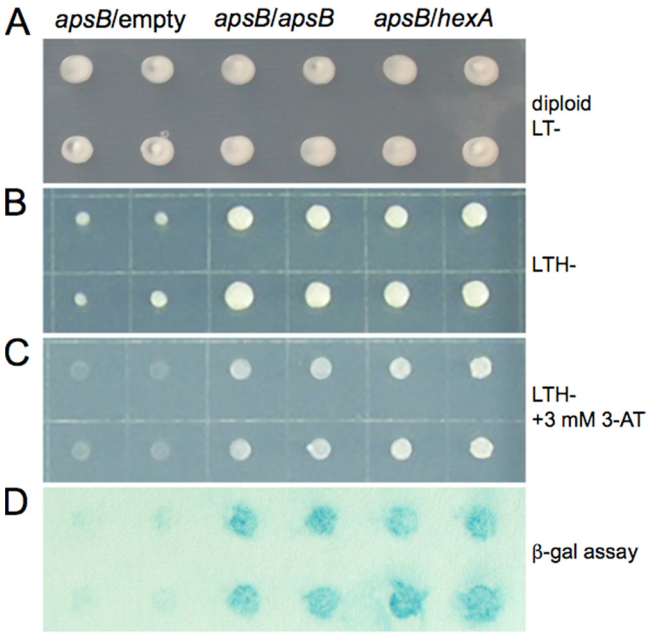

FIG. 3. Interaction of HexA and ApsB in the yeast two-hybrid system. (A) After crossing of Y2HapsB-BD with pGAD424 (empty vector), Y2HapsB-AD (*apsB*), or Y2HhexA-AD (*hexA*), diploids were grown on YEPD agar lacking leucine and tryptophan. Four colonies of each strain are shown for each combination. From here, colonies were inoculated onto selective YEPD medium lacking leucine, tryptophan, and histidine, which supports growth only in the case of interaction (B). (C) The same as in panel B but with the addition of 3 mM 3-AT to reduce background growth. (D) β-Gal assay of the colonies shown in panel A.

had about 95% hits, ApsB and AcuE showed only 14% colocalization, indicating that ApsB was transported only to a subclass of peroxisomes. In addition, we determined the frequency of mRFP1-ApsB and GFP-HexA colocalization to 10% (Fig. 4C). Similar results were obtained with *S. macrospora*, where Pro40 also colocalized only partially with HexA (5). An interaction between ApsB and HexA in *A. nidulans* was also shown *in vivo* using the BiFC assay system in strains coexpressing the N-terminal half of YFP (YN) fused to *hexA* and the C-terminal half of YFP (YC) fused to *apsB* or the other way around (Fig. 4D). ApsB-HexA colocalizing spots were found in the cytoplasm and at some septa (10%). To obtain a clearer picture of the ApsB and HexA structures at septa, we used deconvolution and laser-scanning spinning-disc microscopy. ApsB appeared normally as two spots in the center of the septal pore, whereas HexA localized normally on each side of the pore (Fig. 5). In three-dimensional (3D) reconstruction pictures, the spots appeared with a longer shape along the rim of the septum. Time course experiments revealed that ApsB colocalized with the constricting ring during septation (Fig. 6). These data show that at septa ApsB does not localize to peroxisomes or the Woronin body but rather the putative MTOC is embedded in the membrane of the septal pore.

Mutation of the peroxisomal target sequence in ApsB leads to HexA-like localization at septa. In order to test the functionality of the PTS2 sequence in ApsB, we mutated the consensus sequence ($Q^{73}L$ and $L^{74}R$) and fused the modified ApsB protein with GFP (pDV43). The construct (GFP-

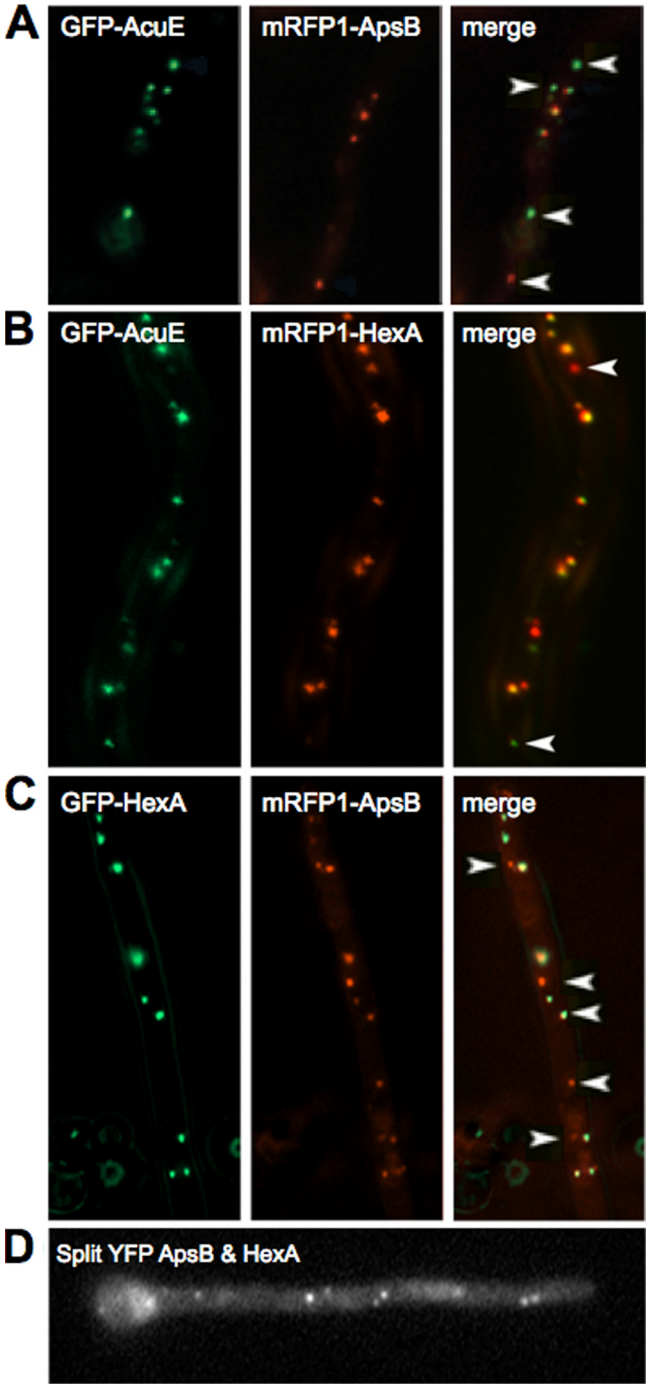

FIG. 4. ApsB localizes to a subclass of peroxisomes. (A) mRFP1-ApsB colocalized with GFP-AcuE, a peroxisomal enzyme, at a frequency of 14%, while the remaining 86% did not colocalize (arrowheads). The strain is SDV70b. (B) mRFP1-tagged HexA colocalized with GFP-tagged AcuE (SDV78c) in 95%. Only 5% of the spots were either GFP or mRFP1 labeled (arrowheads). (C) Colocalization of GFP-HexA and mRFP1-ApsB (SDV49-4). The frequency of colocalization was about 10%. (D) Bimolecular fluorescence complementation assay of HexA and ApsB (strain SDV42). Identical results were obtained with strain SDV43.

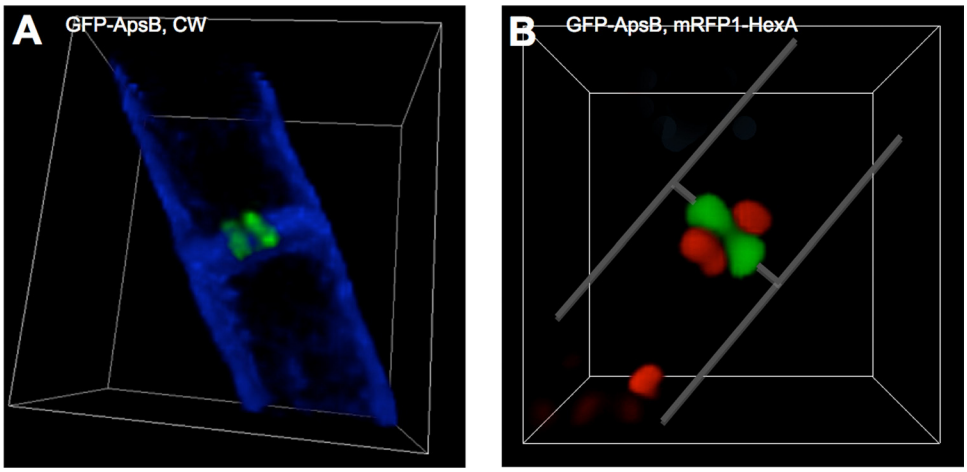

FIG. 5. Comparison of the septal localization of ApsB and HexA. (A) GFP-ApsB appeared as two spots in the center of the septal pore. The cell wall (CW) was stained with Calcofluor white M2R (fluorescent brightener 28 [F3543]; Sigma-Aldrich, Munich, Germany) at a 1:1,000 dilution for 5 min. A 3D view was captured with Zeiss AxioImager Z1 and AxioVision software (V4.5). (B) Double staining of ApsB and HexA. GFP-ApsB appeared as two spots in the center of the septal pore, whereas HexA localized on each side of the pore (three spots in the image). The cell wall is indicated by a line. A 3D view was captured with a Zeiss Cell Observer SD confocal microscope and AxioVision software (V4.5). The strains are SEa3 (A) and SDV73 (B).

ApsB_PTS2^{mut}) was first transformed into wild-type *A. nidulans* strain TN02A3 (resulting in SDV77) and then introduced into strains in which either *hexA* was deleted (SDV79) or *apsB* was mutated (SDV80) or both *hexA* and *apsB* were deleted (SDV95). In strain SDV77, the localization pattern of GFP-ApsB_PTS2^{mut} at SPBs and at cytoplasmic spots looked like that of wild-type GFP-ApsB (Fig. 7A). However, it was surprising to find that the localization of GFP-ApsB_PTS2^{mut} at septa (Fig. 7C) did not show the normal localization of GFP-ApsB (Fig. 7B) but resembled in 70% of the cases the pattern of GFP-HexA (Fig. 7D), whereas in 22% of the cases it was similar to the GFP-ApsB localization. These localization patterns could be achieved through a piggyback import mechanism of GFP-ApsB_PTS2^{mut} along with HexA or ApsB, which were still present as fully functional proteins in SDV77. Only in a strain lacking both ApsB and HexA (SDV95), the specific localization of the mutated ApsB protein was lost at septa (Fig. 7E). The results obtained with the last strain clearly argue for a role for peroxisomes in the transport of ApsB to septal MTOCs. It remains to be elucidated how the assembly of the MTOC at septa occurs.

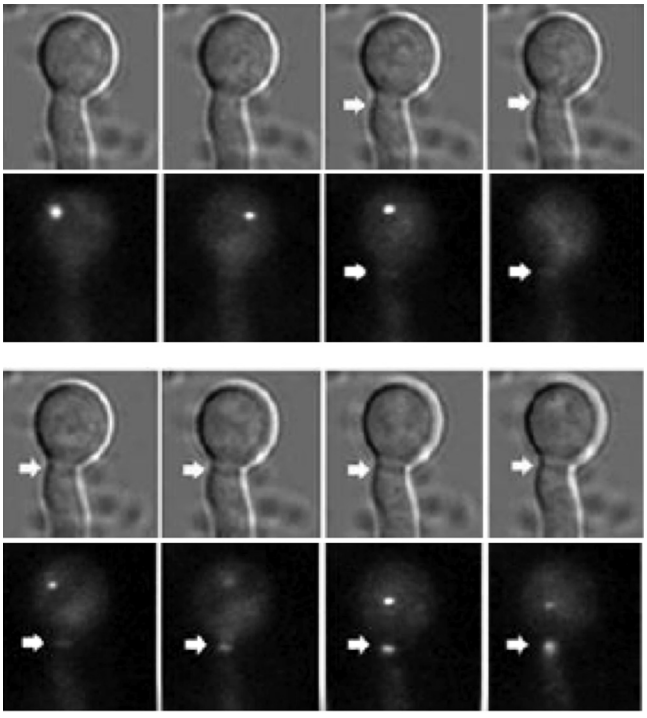

FIG. 6. ApsB follows the constricting ring during septum formation. Time course study of GFP-ApsB in strain SEa3 during septation. The pictures shown were taken at 5-min intervals.

The PTS2 motif of ApsB is important for asexual spore formation. To test whether the altered localization pattern of GFP-ApsB_PTS2^{mut} at septa prevents its biological function, we analyzed if the mutated ApsB protein is able to complement the oligosporogenic phenotype produced by an *apsB* mutation. Therefore, we transformed ApsB [*alcA*(*p*)::*GFP*::*apsB*] and the PTS2-mutated ApsB protein (GFP-ApsB_PTS2^{mut}) into strain AJC1.5 (*apsB6*). Under repressing conditions (glucose), all three strains showed brown colonies, due to the reduced numbers of spores, which is typical for *apsB* mutant strains (4, 32). Under inducing conditions (glycerol or sorbitol), however, wild-type ApsB protein was able to complement the oligosporogenic phenotype (spores were produced), while PTS2-mutated ApsB did not complement it (Fig. 8A and B).

As we previously described, ApsB is important for the production of MTs at sMTOCs (35). Therefore, we wanted to know if the failure of PTS2-mutated ApsB to complement the oligosporogenic phenotype was due to an inability to restore the MTOC activity at septa. In a GFP-ApsB_PTS2^{mut} strain with GFP-labeled MTs and an *apsB6* background, the number of MTs was similar to the number of MTs in *apsB* mutant strains (data not shown). Therefore,

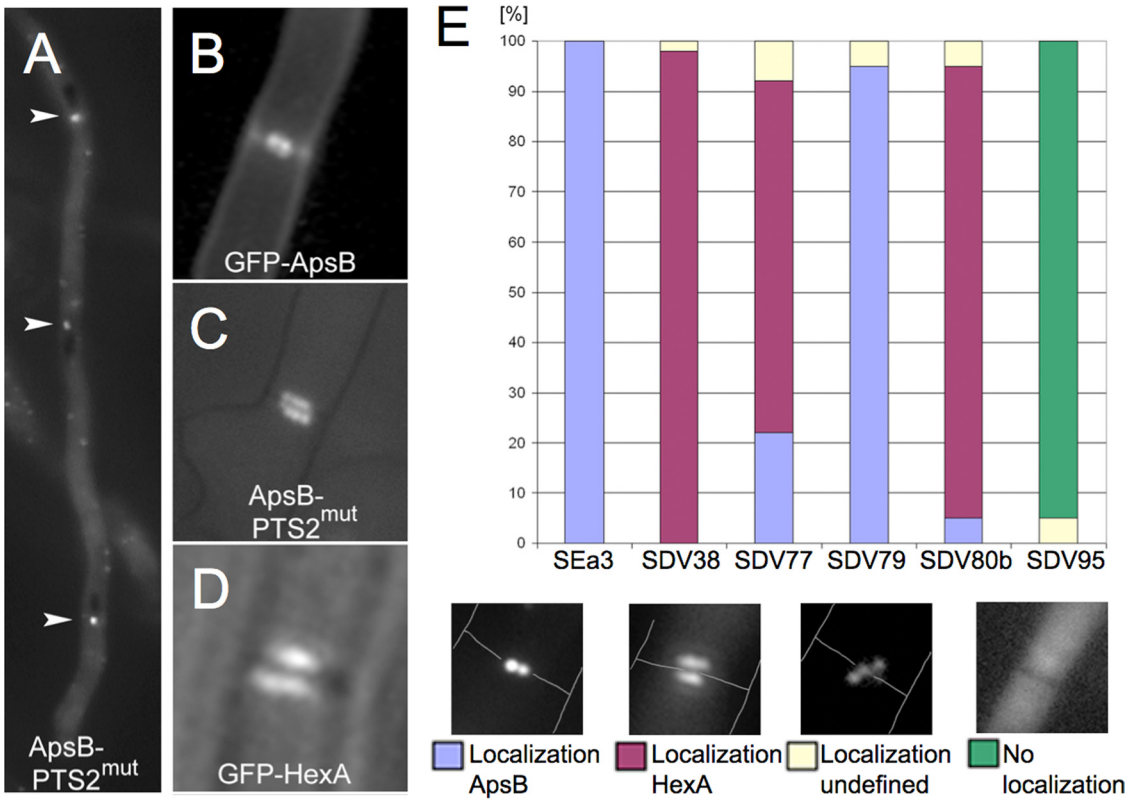

FIG. 7. Mutagenesis of PTS2 of ApsB. (A) GFP-ApsB_PTS2^{mut} localized to SPBs (arrowheads) and to cytoplasmic spots in SDV77 (genotype). At septa, the localization pattern resembled the pattern of GFP-ApsB or GFP-HexA, depending on the genetic background (B to E). (B) GFP-ApsB in the wild type (SEa3). (C) ApsB-PTS2^{mut} in SDV 77. (D) GFP-HexA in the wild type (SDV38). (E) Quantification of septal localization patterns. We determined the localization patterns of GFP-ApsB_PTS2^{mut} in the presence of a wild-type copy of ApsB and in the absence of HexA (SDV79), in the presence of a wild-type copy of HexA and a mutated copy of ApsB (*apsB6*) (SDV80b), in the presence of both proteins (SDV77), or in the absence of both proteins (SDV95). The pictures illustrate the localization patterns.

we assume that PTS2 of ApsB is important for its function at septa.

Next we tested if the function of PTS2-mutated ApsB can be restored by adding a PTS1 targeting sequence (SRL) at the C terminus of ApsB. We transformed PTS2-mutated ApsB with the PTS1 signal fused to the C-terminal part of the protein (GFP-ApsB_PTS2^{mut}_SRL) expressed from the *alcA* promoter into strain AJC1.7 (*apsB10*), resulting in SNZ34, and into *apsB* deletion strain (SRS24), resulting in SNZ94. The *apsB10* mutation converts codon 83 into a stop codon, and thus the mutant lacks most of the 1,052-amino-acid-long ApsB protein (data not shown). The transformed plasmids were integrated ectopically. Transformants of both strains (SNZ34 and SNZ94) appeared with the brown *apsB* mutant-like phenotype under repressing conditions (glucose) and a wild-type-like, spore-producing phenotype under inducing conditions (sorbitol). These results suggest that the ApsB-PTS1 protein was able to complement the developmental phenotype (Fig. 8).

DISCUSSION

In this paper, we show that ApsB interacts with gamma-tubulin at SPBs, at septa, at the tips of growing hyphae, and in spot-like structures in the cytoplasm. This is the first evidence for the presence of gamma-tubulin at septa and in the hyphal tip region. We had evidence before that MTOCs exist at septa, but the nature of these MTOCs remained elusive (35). Our new results show that at least two other proteins associated with nuclear MTOCs exist in septal MTOCs, GcpC and the crucial protein gamma-tubulin. These findings are in agreement with the recent localization of GcpC (40). However, it is still unclear if sMTOCs share more or all proteins with nuclear MTOCs or whether specific proteins exist only at one or the other place. The biggest unsolved question is still the anchorage of sMTOCs. Structurally, the nuclear MTOC of *S. cerevisiae* has been studied the best and recently similar results were obtained with *A. gossypii* (14, 18, 19). It is likely that the situation is similar in *A. nidulans* and that nuclear MTOCs are embedded in the nuclear envelope. However, structural information about sMTOCs is still missing. Our fluorescence microscopy studies indicate that the MTOC appears as two dots inside the septal rim. The structure is clearly different from that of Woronin bodies at septa. Sometimes the two ApsB dots appeared to be connected through a third small dot. This has been described before in *S. pombe* for the equatorial MTOCs (eMTOCs), which are also characterized by the ApsB-homologous protein mto1 (formerly named mod20 or mbo1) (10, 29). In this yeast species, MTs are generated from nuclear MTOCs, eMTOCs, and interphase MTOCs (10, 28). The importance of

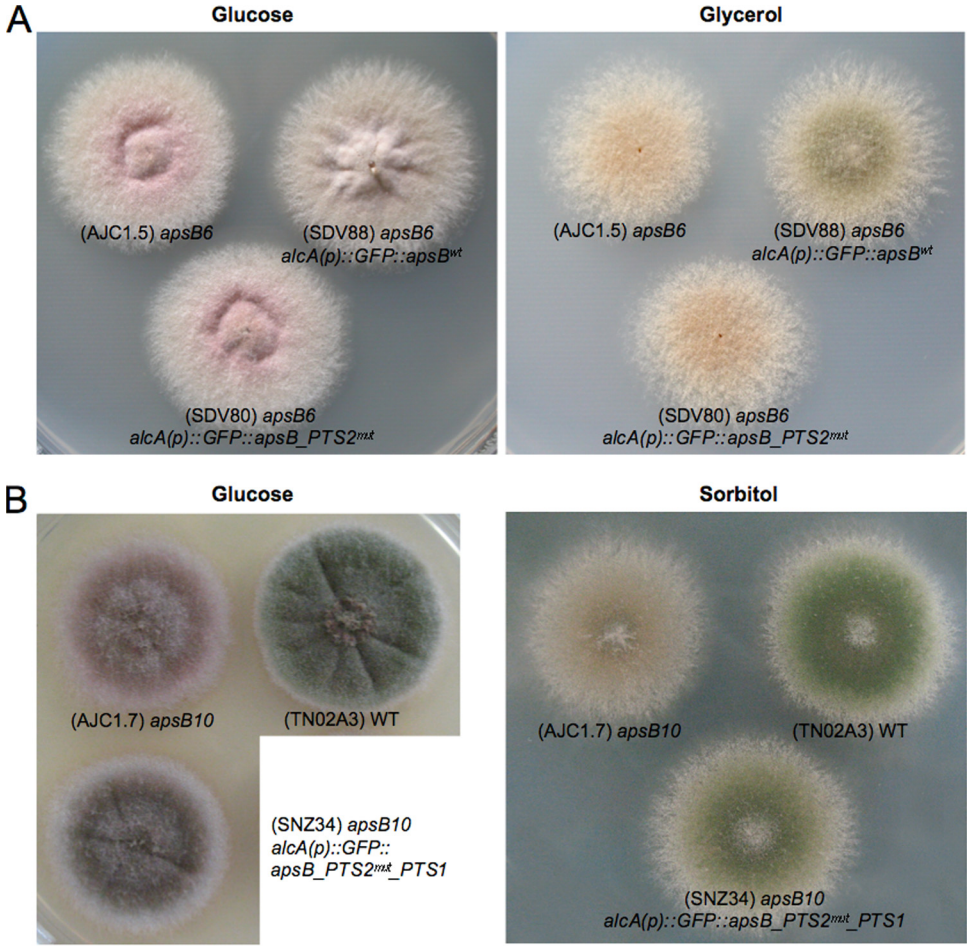

FIG. 8. The peroxisomal target sequence of ApsB is important for complementation of the oligosporogenic phenotype of *apsB* mutants. (A) Transformation of an *apsB6* mutant strain with wild-type *apsB* or the mutated *apsB* forms (strains SDV88 and SDV80, respectively). The constructs were expressed from the *alcA* promoter. It is repressed on glucose and derepressed on glycerol. (B) Transformation of an *apsB10* mutant strain with a mutated version of *apsB* in which a PTS1 sequence was added at the C terminus. Wild-type (WT) strain TN02A3, an *apsB* mutant strain (AJC1.7, *apsB10*), and the transformed strain (SNZ34) were grown on glucose and under inducing conditions on sorbitol.

non-nucleus-associated MTOCs was nicely demonstrated in enucleate cells (3).

We also identified the ApsB–gamma-tubulin interaction in the tips of growing hyphae. This is also the first evidence for gamma-tubulin in the hyphal tip. In comparison, in the chytridiomycete *Allomyces macrogynus*, gamma-tubulin has been identified as a component of the Spitzenkörper (21). Further evidence that gamma-tubulin may be functional in the hyphal tip comes from our observation that some MTs emanate from the hyphal tip and grow into the cytoplasm (16). We speculated at the time that either MTs which did not stop growth after reaching the hyphal tip or MT fragments close to the hyphal tip could be the origin of polymerization. However, our new results point to the possibility that MTOCs exist in the apical region of the hypha.

Several lines of evidence show that the spot-like appearance of ApsB and the ApsB–gamma-tubulin interaction are due to peroxisomal localization: colocalization with AcuE and HexA and the drastic reduction of the number of cytoplasmic spots in a *pexC* mutant. One very strong argument is the importance of the PTS2 sequence and the rescue of the PTS2 mutation by the addition of a PTS1 sequence to the C terminus. The nonfunctionality of ApsB with a mutated PTS2 sequence could still be explained by the fact that this region appears to be evolutionarily conserved from yeast to humans (29), but the rescue of the mutation by the addition of the PTS1 sequence speaks clearly against this possibility. We envisage three possible explanations for the role of the peroxisomal localization. (i) Peroxisomes serve as hosts for sMTOCs. (ii) Peroxisomes catalyze a reaction that is required for MTOC function at the septum and is ApsB dependent. (iii) Peroxisomes serve as transport vehicles for sMTOC-associated proteins. Our results point to a transport function for peroxisomes. In agreement with such a role is the observation of fast-moving mto1 (ApsB) spots in *S. pombe* (29). These structures could represent peroxisomes. However, many open questions remain to be solved, e.g., how the proteins are further recruited from the peroxisomes to the sMTOCs. Against all three possibilities speaks the observation that the septal localization of ApsB and sMTOC function in mutants with defects in PTS1 or PTS2 peroxisomal protein import or in *pexC* mutants lacking peroxisomes appeared sim-

ilar to the situation in the wild type (results not shown). However, it has to be considered that the *pexC* mutant strain displays pleiotropic phenotypes and that the possibility of a piggyback import mechanism might mask the possible effects of PTS1 or PTS2 defects (12).

From our results we conclude that ApsB defines a new class of peroxisomes that is—besides the Woronin bodies—the second example of peroxisomes as organelles with a function beyond metabolic pathways (30).

ACKNOWLEDGMENTS

We are grateful to M. Hynes (University of Melbourne, Melbourne, Australia) for sending us peroxisomal marker proteins and *pex* mutant strains and to G. Jedd for helpful discussions and the *hexA* deletion strains. We thank R. Suelmann, Björn Titz, and Sabrina Hettinger for initial help with this project.

The work was funded by the Deutsche Forschungsgemeinschaft, the Fonds der Chemischen Industrie, and the special program Lebensmittel und Gesundheit of the Landesstiftung Baden Württemberg. N.Z. was partly supported by a fellowship from the Syrian ministry.

REFERENCES

1. **Buller, A. H. R.** 1931. Researches on fungi. Hafner Publishing Co., New York, NY.
2. **Cagney, B., P. Uetz, and S. Fields.** 2000. High-throughput screening for protein-protein interactions using the two-hybrid assay. Methods Enzymol. **328:**3–14.
3. **Carazo-Salas, R. E., and P. Nurse.** 2006. Self-organization of interphase microtubule arrays in fission yeast. Nat. Cell Biol. **8:**1102–1107.
4. **Clutterbuck, A. J.** 1994. Mutants of *Aspergillus nidulans* deficient in nuclear migration during hyphal growth and conidiation. Microbiology **140:**1169–1174.
5. **Engh, I., C. Würtz, K. Witzel-Schlömp, H. Y. Zhang, B. Hoff, M. Nowrousian, H. Rottensteiner, and U. Kück.** 2007. The WW domain protein PRO40 is required for fungal fertility and associates with Woronin bodies. Eukaryot. Cell **6:**831–843.
6. **Gabaldón, T., B. Snel, F. van Zimmeren, W. Hemrika, H. Tabak, and M. A. Hyunen.** 2006. Origin and evolution of the peroxisomal proteome. Biol. Direct **1:**8.
7. **Gould, S. J., G. A. Keller, N. Hosken, J. Wilkinson, and S. Subramani.** 1989. A conserved tripeptide sorts proteins to peroxisomes. J. Cell Biol. **108:**1657–1664.
8. **Hayashi, M., and M. Nishimura.** 2003. Entering a new era of research on plant peroxisomes. Curr. Opin. Plant Biol. **6:**577–582.
9. **Heiland, I., and R. Erdmann.** 2005. Biogenesis of peroxisomes. FEBS J. **272:**2362–2372.
10. **Heitz, M. J., J. Petersen, S. Valovin, and I. M. Hagan.** 2001. MTOC formation during mitotic exit in fission yeast. J. Cell Sci. **114:**4521–4532.
11. **Hill, T. W., and E. Käfer.** 2001. Improved protocols for *Aspergillus* minimal medium: trace element and minimal medium salt stock solutions. Fungal Genet. Newsl. **48:**20–21.
12. **Hynes, M. J., S. L. Murray, G. S. Khew, and M. A. Davis.** 2008. Genetic analysis of the role of peroxisomes in the utilization of acetate and fatty acids in *Aspergillus nidulans*. Genetics **178:**1355–1369.
13. **James, P., J. Halladay, and E. A. Craig.** 1996. Genomic libraries and a host strain designed for highly efficient two-hybrid selection in yeast. Genetics **144:**1425–1436.
14. **Jaspersen, S. L., and M. Winey.** 2004. The budding yeast spindle pole body: structure, duplication, and function. Annu. Rev. Cell Dev. Biol. **20:**1–28.
15. **Jedd, G., and N.-H. Chua.** 2000. A new self-assembled peroxisomal vesicle required for efficient resealing of the plasma membrane. Nat. Cell Biol. **2:**226–231.
16. **Konzack, S., P. Rischitor, C. Enke, and R. Fischer.** 2005. The role of the kinesin motor KipA in microtubule organization and polarized growth of *Aspergillus nidulans*. Mol. Biol. Cell **16:**497–506.
17. **Kovacs, W. J., S. Krisans, S. Hogenboom, R. J. Wanders, and H. R. Waterham.** 2003. Cholesterol biosynthesis and regulation: role of peroxisomes. Adv. Exp. Med. Biol. **544:**315–327.
18. **Lang, C., S. Grava, M. Finlayson, R. Trimble, P. Philippsen, and S. L. Jaspersen.** 2010. Structural mutants of the spindle pole body cause distinct alterations of cytoplasmic microtubules and nuclear dynamics in multinucleated hyphae. Mol. Biol. Cell **21:**753–766.
19. **Lang, C., S. Grava, T. van den Hoorn, R. Trimble, P. Philippsen, and S. L. Jaspersen.** 2010. Mobility, microtubule nucleation and structure of microtubule-organizing centers in multinucleated hyphae of *Ashbya gossypii*. Mol. Biol. Cell **21:**18–28.
20. **Maruyama, J., P. R. Juvvadi, K. Ishi, and K. Kitamoto.** 2005. Three-dimensional image analysis of plugging at the septal pore by Woroinin body during hypotonic shock inducing hyphal tip bursting in the filamentous fungus *Aspergillus oryzae*. Biochem. Biophys. Res. Commun. **331:**1081–1088.
21. **McDaniel, D. P., and R. W. Roberson.** 1998. γ-Tubulin is a component of the Spitzenkörper and centrosomes in hyphal-tip cells of *Allomyces macrogynus*. Protoplasma **203:**118–123.
22. **Momany, M., E. Richardson, C. Van Sickle, and G. Jedd.** 2002. Mapping Woronin body position in *Aspergillus nidulans*. Mycologia **94:**260–266.
23. **Nayak, T., E. Szewczyk, C. E. Oakley, A. Osmani, L. Ukil, S. L. Murray, M. J. Hynes, S. A. Osmani, and B. R. Oakley.** 2006. A versatile and efficient gene targeting system for *Aspergillus nidulans*. Genetics **172:**1557–1566.
24. **Osmani, A. H., J. Davies, C. E. Oakley, B. R. Oakley, and S. A. Osmani.** 2003. TINA interacts with the NIMA kinase in *Aspergillus nidulans* and negatively regulates astral microtubules during metaphase arrest. Mol. Biol. Cell **14:**3169–3179.
25. **Purschwitz, J., S. Müller, and R. Fischer.** 2009. Mapping the interaction sites of *Aspergillus nidulans* phytochrome FphA with the global regulator VeA and the white collar protein LreB. Mol. Genet. Genomics **281:**35–42.
26. **Raynaud-Messina, B., and A. Merdes.** 2007. Gamma-tubulin complexes and microtubule organization. Curr. Opin. Cell Biol. **19:**24–30.
27. **Sambrook, J., and D. W. Russell.** 2001. Molecular cloning: a laboratory manual, 3rd ed. Cold Spring Harbor Laboratory Press, Cold Spring Harbor, NY.
28. **Samejima, I., P. C. C. Laurenco, H. A. Snaith, and K. E. Sawin.** 2005. Fission yeast mto2p regulates microtubule nucleation by the centrosomin-related protein mto1p. Mol. Biol. Cell **16:**3040–3051.
29. **Sawin, K. E., P. C. C. Lourenco, and H. A. Snaith.** 2004. Microtubule nucleation at non-spindle pole body microtubule-organizing centers requires fission yeast centrosomin-related protein mod20p. Curr. Biol. **14:**763–775.
30. **Schrader, M., and H. D. Fahimi.** 2008. The peroxisome: still a mysterious organelle. Histochem. Cell Biol. **129:**421–440.
31. **Suelmann, R., N. Sievers, and R. Fischer.** 1997. Nuclear traffic in fungal hyphae: *in vivo* study of nuclear migration and positioning in *Aspergillus nidulans*. Mol. Microbiol. **25:**757–769.
32. **Suelmann, R., N. Sievers, D. Galetzka, L. Robertson, W. E. Timberlake, and R. Fischer.** 1998. Increased nuclear traffic chaos in hyphae of *apsB* mutants of *Aspergillus nidulans*: molecular characterization of *apsB* and *in vivo* observation of nuclear behaviour. Mol. Microbiol. **30:**831–842.
33. **Swinkels, B. W., S. J. Gould, A. G. Bodnar, R. A. Rachubinski, and S. Subramani.** 1991. A novel, cleavable peroxisomal targeting signal at the amino-terminus of the rat 3-ketoacyl-CoA thiolase. EMBO J. **10:**3255–3262.
34. **Toews, M. W., J. Warmbold, S. Konzack, P. E. Rischitor, D. Veith, K. Vienken, C. Vinuesa, H. Wei, and R. Fischer.** 2004. Establishment of mRFP1 as fluorescent marker in *Aspergillus nidulans* and construction of expression vectors for high-throughput protein tagging using recombination in *Escherichia coli* (GATEWAY). Curr. Genet. **45:**383–389.
35. **Veith, D., N. Scherr, V. P. Efimov, and R. Fischer.** 2005. Role of the spindle-pole body protein ApsB and the cortex protein ApsA in microtubule organization and nuclear migration in *Aspergillus nidulans*. J. Cell Sci. **118:**3705–3716.
36. **Wanders, R. J.** 2004. Metabolic and molecular basis of peroxisomal disorders: a review. Am. J. Med. Genet. **126A:**355–375.
37. **Wanders, R. J., and H. R. Waterham.** 2006. Biochemistry of mammalian peroxisomes revisited. Annu. Rev. Biochem. **75:**295–332.
38. **Waring, R. B., G. S. May, and N. R. Morris.** 1989. Characterization of an inducible expression system in *Aspergillus nidulans* using *alcA* and tubulin coding genes. Gene **79:**119–130.
39. **Woronin, M.** 1864. Entwicklungsgeschichte der *Ascobolus pucherrimus* Cr. und einiger Pezizen. Abh. Senkenb. Naturforsch. **5:**333–344.
40. **Xiong, Y., and B. R. Oakley.** 2009. *In vivo* analysis of the functions of gamma-tubulin-complex proteins. J. Cell Sci. **122:**4218–4227.
41. **Yelton, M. M., J. E. Hamer, and W. E. Timberlake.** 1984. Transformation of *Aspergillus nidulans* by using a *trpC* plasmid. Proc. Natl. Acad. Sci. U. S. A. **81:**1470–1474.
42. **Yuan, P., G. Jedd, D. Kumaran, S. Swaminathan, H. Shio, D. Hewitt, N.-H. Chua, and K. Swaminathan.** 2003. A Hex-1 crystal lattice required for Woronin body function in *Neurospora crassa*. Nat. Struct. Biol. **10:**264–270.